Spontaneous rotational Raman thermometry for air flow characterization in a turbomachine test rig

Michael Scherman, Rosa Santagata, Jean Pierre Faleni, Mikaël Orain, Alexandre Bresson, Brigitte Attal-tretout, Alexander Krumme

Spontaneous rotational Raman thermometry for air flow characterization in a turbomachine test rig.

Michael SCHERMAN[1], Rosa SANTAGATA[1], Jean Pierre FALENI[1], Mikael ORAIN[2],

Alexandre BRESSON[1], Brigitte ATTAL-TRETOUT[1], Alexander KRUMME[3].

[1] ONERA, Chemin de la Hunière BP 80100, 91123 Palaiseau

[2] ONERA, Route de Mauzac, 31410 Mauzac

[3] DLR, Institute of Propulsion Technology, Bunsentr 10, 37073 Göttingen

michael.scherman@onera.fr

Abstract

Non-invasive and accurate measurements are essential to study the reactive flows in aeronautical engines. This paper reports the results of a unique measurement campaign providing the temperature flowfield in a large scale facility turbomachine test rig using spontaneous rotational Raman scattering technique. Different planes of interest and operating conditions are probed, showing good agreement with thermocouple measurements. Fast temperature variations (>7.7 kHz) could be probed thanks to synchronization of the laser pulse with the rotor clock. Results outline the performance of *in situ* Raman technique to investigate steady and unsteady flows in turbine's conditions.

Keywords*:* Raman spectroscopy, Thermometry, Turbomachine, Spontaneous Raman scattering, laser diagnostics

1. INTRODUCTION

Accurate flow field measurements are essential to fully understand the phenomena involved in aeronautical engines. Quantitative measurements in those harsh environments are required to evaluate the ability of the computational fluid dynamics (CFD) simulations in order to predict the behavior of the engine in operation. Significant trust in simulation predictions is indeed necessary to reduce conception and optimization costs[1]. For instance, appropriate design and assembly of the system components, and the knowledge of their influence on the flowfield behavior, are required to maximize the engine total efficiency. Among other variables, temperature is a key parameter to describe the flow. Its knowledge requires a temporally and spatially resolved nonintrusive thermometry method to be accurate.

In the last years, advances in laser-based diagnostic tools for combustion and aerospace research have led to great achievements in flow field measurements like species detection and tomographic imaging[2]. Indeed, optical techniques are well suited since they do not perturb the flow, whereas traditional techniques do (thermocouples, hot wire), if optical accesses allow light propagation toward the measurement volume. They also have higher bandwidths (up to MHz) than thermocouples (up to kHz) and allow observing the fast evolution of the flow (kHz-MHz). However the presence of soot, temperature gradients and wall vicinity in highly turbulent environments constitutes a challenge for measurement. Among laser-based

diagnostics, Raman scattering is sensitive over a wide temperature range and is able to provide space and time-resolved measurements in those media.

Spontaneous Raman scattering (SRS) is one of the most established spectroscopic technique [3,4,5], it has been proven for gas phase thermometry[6] and it has been widely used in probing turbulent flames. Simultaneous measurement of temperature as well as the concentration of most of the major combustion species can be achieved, while using only a single excitation laser beam. This relatively simple optical setup makes this technique very reliable and robust in harsh environments where vibrations and acoustic noise have to be faced. This is particularly discriminatory as compared to coherent other techniques such as anti-Stokes Raman scattering (CARS) or laser-induced grating scattering (LIGS) that suffer from misalignments issues since three beams have to precisely overlap to perform the measurement, or Rayleigh scattering that requires very precise calibration procedures. SRS also takes benefits of back scattering capability in order to probe media with a single optical window which is a clear advantage in industrial applications and helps to minimally perturb the flow.

SRS results from inelastic interaction between light and matter. Incoming light is scattered by a molecular medium with a frequency shift characteristics of the vibrational and rotational molecular energy. The temperature can be measured from the relative line amplitudes of the Raman spectrum since a Boltzmann distribution drives the population of the ro-vibrational manifold of levels. Spontaneous rotational Raman scattering (SR2S) is the study of the molecular rotational lines at small wavenumbers (0-500 cm^{-1}), and is well adapted to temperature measurement below 1000 K[7], as often encountered in turbomachinery flows. SRS is traditionally used for measurement in stationary media since it requires long acquisition times (seconds to minutes) due to weakness of the Raman cross section. Single shot capability of spontaneous Raman thermometry has also been demonstrated[8,9] using high energy pulsed lasers (~500 mJ/pulse). However, they operate at low repetition rate (~10 Hz), and are unable to probe fast temporal dynamics. The accuracy of SR2S technique was shown to be very good at ambient temperature. For example, Drake et al.[10] have mentioned an accuracy of ±2 K at about 300 K using signal accumulation over 45 s, and ~2.2% in single shot by Locke et al[8]. In the past, among various applications, SR2S has been used for temperature measurements in flames[11,12,13] and in the atmosphere[14,15,16]. In particular, this technique was applied to thermometry in a high-velocity turbulent jet[8], in a gas turbine model combustor at elevated pressure[17], in a confined swirling natural gas/air flame[18] in high-pressure fuel-rich H_2-air flames[19], as well as in the UV range for imaging of a JetA-fueled aircraft combustor. In the latter, it has been used also as a complementary tool to CARS[20,21] and laser Doppler velocimetry[22]. By synchronizing the laser pulse on a cyclic event, temporal information may be obtained in the flow. The possibility to achieve temperature measurements with 1 K absolute accuracy over 300-600 K[7] was previously demonstrated at Onera in a transonic compressor.

This work reports the use of SR2S for air thermometry in a turbomachine test rig. A peculiarity of aero-engine studies is that it is important to investigate the whole system, composed by the combustor and the turbine, rather than separate modules[23]. The physics of

combustor-turbine interaction is not yet fully understood. This interface is characterized by extreme phenomena like hot gases, unstable boundary layers, turbulence effects and inherent unsteadiness [24,25]. Due to the complexity of the flow and the mechanical access restrictions, measurement is challenging. In our case, a specific test facility[26,27] was designed and assembled at DLR Göttingen during the EC FP7 project FACTOR (Full Aerothermal Combustor-Turbine interactiOns Research). It consists of a combustor simulator coupled to a high-pressure turbine. The combustor simulator injects a 3.09 kg/s total mass flow of hot air (>513 K) through 20 swirlers periodically located over the annular chamber (18° periodicity). In the combustor simulator chamber, the hot air is mixed to effusion coolant mass flow (1.62 kg/s) extracted from the inner and outer liner on the circumference. The total mass of 4.71 kg/s then flows through the turbine in which stator contains 40 blades (9° periodicity) and the rotor 60 blades (6° periodicity). The rotor turbine (395 kW) is operated at 7700 rotations per minute. Further details and illustrations of the rig are given in the Supporting Information.

The results of the measurement campaign carried out at DLR Göttingen NG-Turb test turbine facility using Raman hyperspectral imaging for flow field characterization are presented. Our system has been successfully used to characterize the flow of this unique test rig. The influence of the rig mechanical configuration on the flow field has been observed. It provides a good dataset to be compared and to validate numerical codes, and it is also a key feature to measure the experimental efficiency of the turbomachine. It may also be used to produce a generic set of guidelines in order to model combustor-turbine interaction.

2. MATERIAL AND METHODS

The Raman setup is illustrated in Fig. 1. A Nd:YAG laser source produces 20 ns duration infra-red pulses at 1064 nm, with a repetition rate tunable between 7 and 14 kHz. A doubling crystal (LBO) enclosed in an oven allows to generate 1 W at 532 nm. The pulse train is synchronized to the rotor clock repetition rate at 7.7 kHz (period τ =130 µs) as illustrated in Fig. S2 (Supporting Information). This allows the relative position of the blade and the laser spot to be maintained fixed during the measurement time in order to perform measurements in the rotating frame of the blades. Each spectrum is integrated over 60 s, i.e. 462 000 laser shots. A delay generator is used to scan the phase between the laser and the rotor clocks.

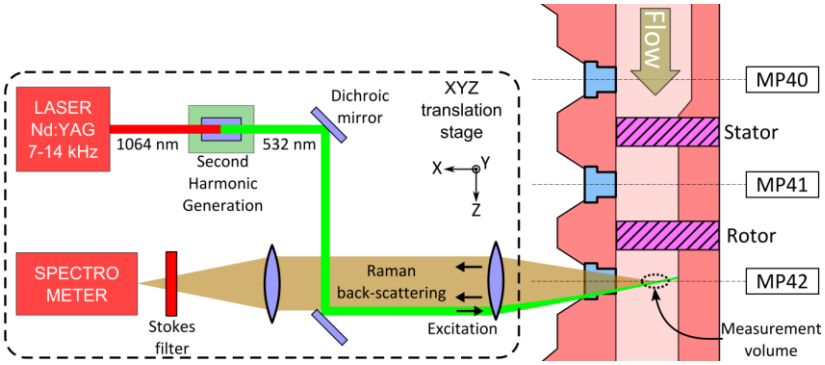

Fig. 1 Scheme of laser excitation, signal collection, and measurement volume at the 3 planes of interest (MP40, MP41, MP42) of the rig.

The laser beam is guided to the rig and focused at the measurement volume through the edge of a 2''-diameter 120 mm-focal length achromatic lens. This lens is also used to collect the Raman backscattered signal. Two interferential filters are used to efficiently reject 532 nm light (due to Mie scattering and stray light) from the collection path. A 750-mm focal length spectrometer is used to record the Stokes spectrum. The dispersive element is a 2400 grooves/mm grating, and the detector is a Peletier-cooled (-30°C) electron multiplied CCD. The whole optical setup is mounted on a single platform, fixed to a 3D motorized translation stage. The measurement point location is thus translated to investigate various planes of interest.

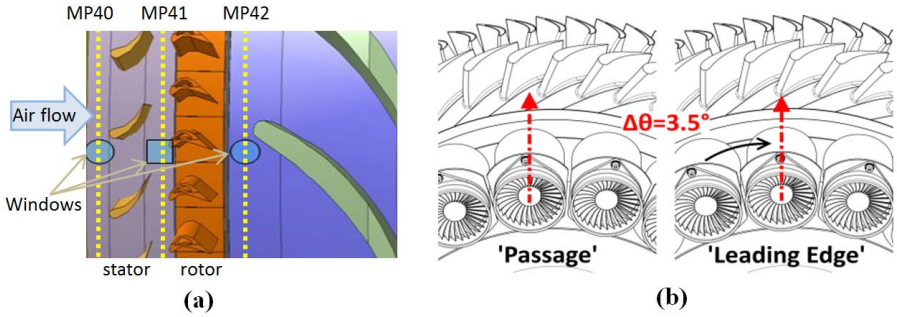

Fig. 2 (a) Drawing of the FACTOR test rig and positions of the measurement planes (MP40, MP41, MP42) upstream from the stator, between the stator and the rotor, and downstream from the rotor. (d) Illustration of the 'Passage' and 'Leading Edge' clocking configurations.

Three planes of interest were investigated as shown in Fig. 2 (a): upstream from the stator (MP40), between the stator and the rotor (MP41) and downstream from the rotor (MP42). Two measurement techniques are applied at the same time to get the temperature field: Raman technique and thermocouple probe. The thermocouple is placed on top of a 5-hole probe head, which provides temperature and Mach Numbers distributions in the scanned area. Raman diagnostic is restricted to a 3° angular range of measurement due to the size of the optical windows. For each plane, two combustor clocking positions were probed, depending on the relative orientation of the swirlers with respect to the static turbine blade rows, as illustrated in Fig. 2 (b). In 'Passage' clocking, combustor swirlers point toward passage of the first stator, while in 'Leading Edge' clocking they point toward the stator leading edges.

In diatomic molecules such as N_2 and O_2, which are major components of the flow in a turbomachine, pure rotational Raman spectrum is retrieved according to selection rules $\Delta v = 0$, and $\Delta J = +2$ for the S branch investigated, where v and J are the vibrational and rotational quantum numbers. Spectral lines are equally spaced according to the expression [4]:

$$\Delta\nu_S(J) = (4B_0 - 6D_0)\left(J + \frac{3}{2}\right) \qquad (1)$$

where $\Delta\nu_S(J)$ is the Raman shift associated with the transition originating from lower level J, and B_0 and D_0 are respectively inertial and centrifugal distortion constants of the molecule (B_0=1.98957 cm^{-1} and D_0=5.76*10^{-6} cm^{-1} for N_2 [5]).

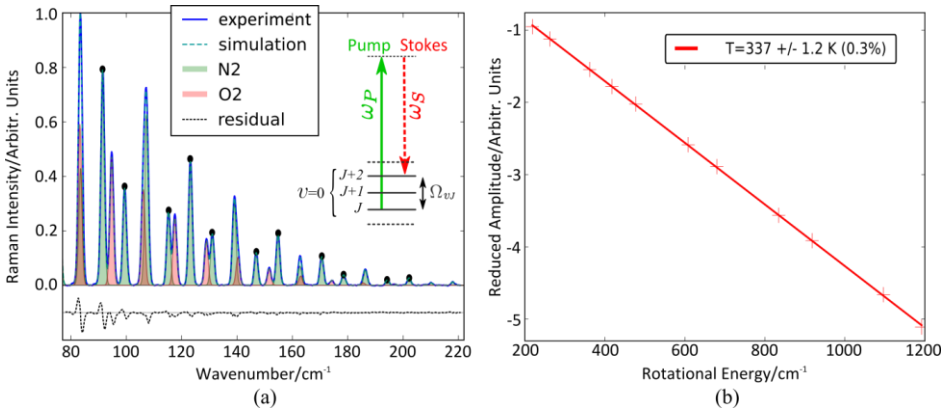

Fig. 3 (a) Typical experimental spectrum (blue) associated with simulated N2 (green) and O2 (red) contributions of the fitted spectrum (dashed turquoise). The residual difference between experimental and calculated profiles is plotted above the horizontal axis (dotted black). Insert: illustration of the Raman Stokes process for a Raman active rotational ($\boldsymbol{J}$) and vibrational ($\boldsymbol{v}$) mode $\boldsymbol{\Omega_{vJ}}$, which fulfils the S branch pure rotational selection rule $\boldsymbol{\Delta J = +2}$. (b) Reduced amplitudes a(J) of the N2 rotational lines as a function of the rotational energy Erot(J) of the lower J level (cross markers), and linear regression calculated to retrieve temperature (solid line).

Typical experimental spectrum is shown Fig. 3 (a) (black curve). A spectrum fitted to the experimental data is shown in dashed turquoise, and the residual between simulated and experimental spectra is plotted in dotted black just above the horizontal axis. Contributions of N_2 (green) and O_2 (red) rotational structures are plotted separately. The spectral resolution of the retrieved spectrum is limited to ~1.2 cm^{-1} FWHM due to the spectrometer. Thus, considering that γ_{N_2}< 0.1 cm^{-1}/bar and 0.5<P<1.5 bar inside the rig, the effect of the pressure on the Raman linewidths has been neglected in the treatment since it is much smaller than the apparatus function.

The temperature measurement is performed according to the procedure described in [7] using a python 2.7 routine. Background rejection and noise filtering is first performed. Then, peak identification is processed to extract position and amplitudes of the N_2 rotational peaks, pointed by the circles in Fig. 4 (a). A threshold is applied to discard peaks having too low signal to noise ratio. Between 8 and 11 peaks are finally used. The reduced peak amplitude is then calculated according to expression:

$$a(J) = \ln\left(\frac{I_J}{S_J}\right) \qquad \textbf{(2)}$$

where I_J is the amplitude of rotational quantum number J peak, and S_J is the normalization coefficient expressed as

$$S_J = g_I \cdot \left(\nu_0 - \nu_S(J)\right)^4 \cdot \frac{3(J+1)(J+2)}{2(2J+3)} \qquad (3)$$

where g_I is the spin degeneracy, ν_0 is the laser wavenumber, $\nu_S(J)$ is the Stokes wavenumber of the rotational line associated to J quantum number. The reduced amplitude $a(J)$ is a linear function of the rotational energy $E_{rot}(J)$, as illustrated in Fig. 3 (b), with a $-1/k_BT$ slope where k_B is the Boltzmann constant and T is the temperature. A linear regression is computed to extract the temperature value using *curve_fit* routine from python/scipy library. The uncertainty σ is provided by the diagonal element of the covariance matrix retrieved from

the fitting routine. Experimental spectra acquired in a laboratory hot air jet demonstrate that σ grows from 2 K to 8 K when temperature increases from 300 K to 800 K, so relative uncertainty σ/T stays below 1 % over the whole range.

For the data acquired in MP42, the post-processing uses a slightly different method to retrieve the temperature. Here, a simulated spectrum has been fitted to the experimental data by adjusting the temperature value. It provides better accuracy since the data, which appear to be noisier in this case, had to be smoothed in a broader window, which distorted the spectral lines and their amplitude distributions.

3. RESULTS AND DISCUSSION

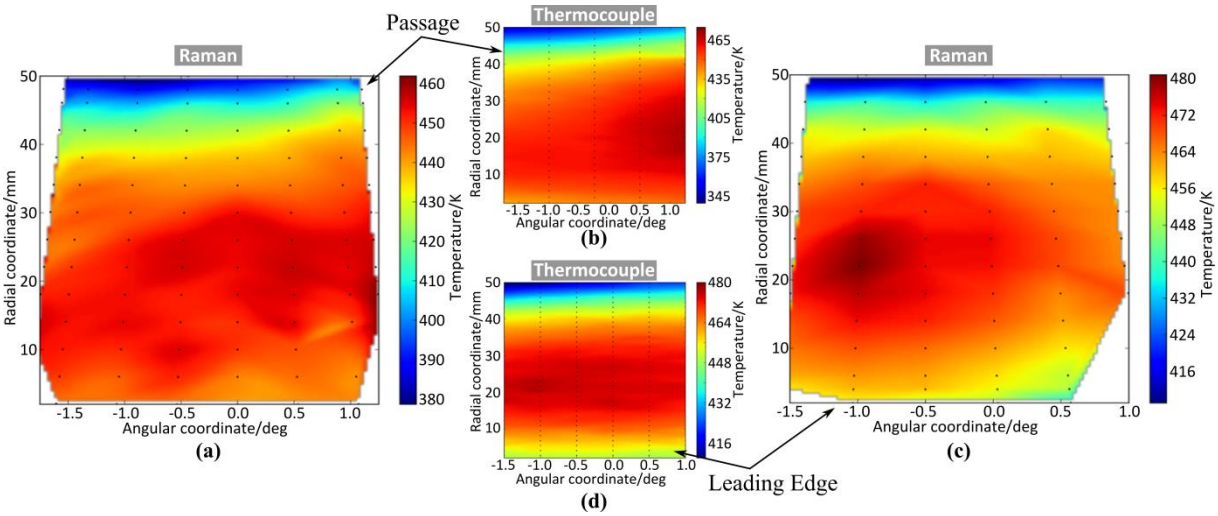

Fig. 4 Temperature maps in MP40 obtained with Raman measurements, for (a) 'Passage', and (c) 'Leading Edge', clocking configurations. Thermocouple measurements are also shown for comparison for (b) 'Passage', and (d) 'Leading Edge', clocking.

Fig. 4 shows the temperature field in MP40 retrieved by Raman for (a) 'Passage' and (c) 'Leading Edge' clocking. Thermocouple measurements are also given for comparison in Fig. 4 (b) and (d). Good agreement is obtained with the two techniques. Similar distribution of the temperature field is obtained, mainly composed of a hot central flow and a cold layer on the walls. Influence of combustor/stator clocking is clearly evidenced although the field of view is restricted (3°). In this plane, the expected clocking effect is mainly a rotation of the flow field of 3.5°. In 'Leading Edge' clocking, the hot pattern signature of the combustor simulators is visible while, in 'Passage' clocking, the Raman window gives access to a region located between two injectors.

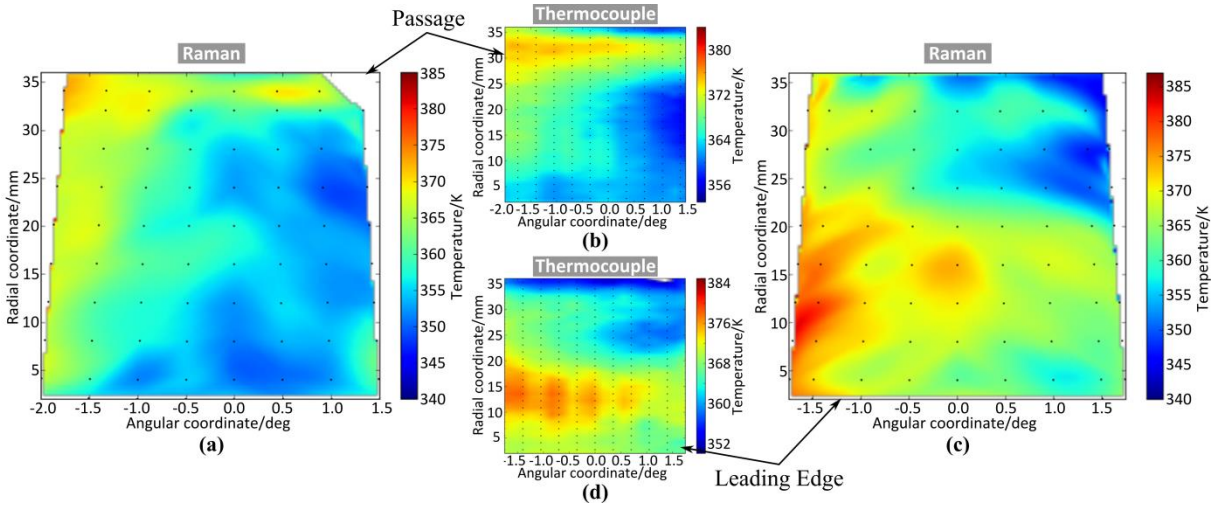

Fig. 5 Temperature maps in MP41 obtained with Raman measurements, for (a) 'Passage', and (c) 'Leading Edge', clocking configurations. Thermocouple measurements are also shown for comparison for (b) 'Passage', and (d) 'Leading Edge', clocking.

Fig. 5 shows the static temperature field retrieved by Raman in MP41 and thermocouple measurements; appropriate corrections due to the Mach number distribution are included (see Supporting Information). Similar spatial temperature profiles are obtained and the influence of combustor/stator clocking is also evidenced. In 'Passage' configuration, a cold structure belonging to one of the 9° spaced bowed trailing edges signatures of the stator is captured in the Raman window. In 'Leading Edge' configuration, the structure of the flow is broken since stator blades are crossing the combustor pattern. The trailing edges cold signature (top-right) is thus hidden due to the presence of a hot spot (bottom-left) attributed to the transportation of hot flow into the passages between the stator blades.

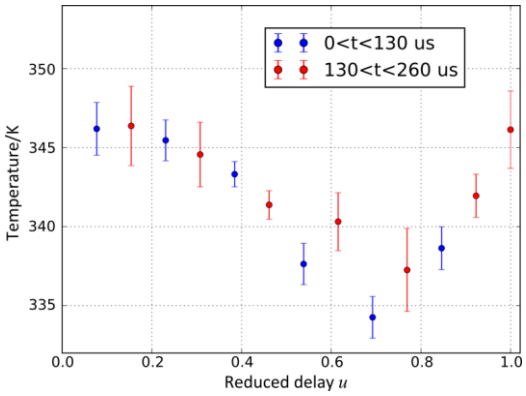

Fig. 6 Evolution of static temperature versus delay between rotor and laser clocks. The delay $\boldsymbol{t}$ was scanned over two periods ($\boldsymbol{\tau = 130}$ µ$\boldsymbol{s}$) by steps of 20 µs. The abscissa of the plot is given in term of dimensionless parameter $\boldsymbol{u = t/\tau}$.

Finally, the temperature field of MP42 is only measured in 'Leading Edge' configuration due to time constraint. To check the ability of the technique to follow unsteady events inside the flow, the temperature is measured at the center of the chamber and the delay t between the laser pulse and the rotor is scanned over two temporal periods (τ =130 µs) by 20 µs steps. A

periodic signal is measured, as illustrated in Fig. 6, confirming that Raman measurements are sensitive to the periodic events induced by the rotation of the rotor. A ~12 K temperature step is estimated over a period.

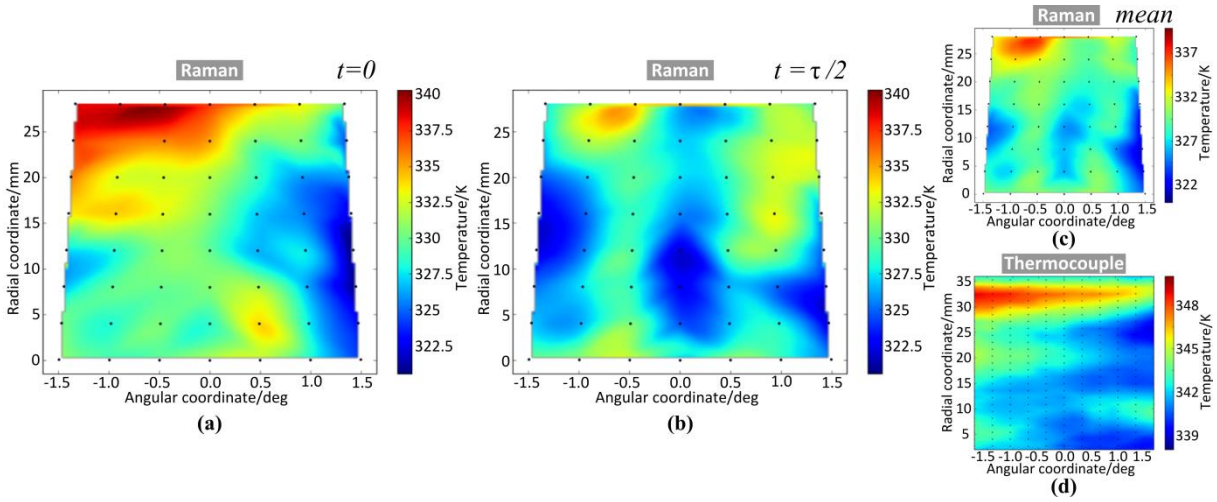

Fig. 7 Raman Temperature maps obtained in MP42 for 'Leading Edge' clocking with (a) zero and (b) $\boldsymbol{\tau}$/2 delay. (c) Average temperature distribution obtained from unsteady Raman measurements and (d) temperature distribution obtained by thermocouple measurements**.**

The temperature maps measured in MP42 are shown in Fig. 7 when the laser clock is (a) synchronised in phase with the rotor clock, and (b) dephased by $\pi/2$, i.e. delayed by $t = 65\ \mu s$. Two different pictures are measured, revealing small structures which differ from the smoother pattern observed in the thermocouple map (Fig. 7 (d)). This is attributed to the instantaneous time sampling capability of Raman probing while thermocouple has slow temporal dynamics, and thus provides measurements in the stationary frame. In particular, a periodic alternation of cold and hot puffs (1.5°) is observed in Fig. 7 (b), corresponding to a periodic signal event in the static frame at 1.925 kHz. This frequency will be compared to unsteady measurements performed with a high speed probe by other project partners, which are still being post-processed. To go further, the average pattern of the two unsteady measurements (Fig. 7 (c)) may be compared to the thermocouple map. Although different on the whole, the two pictures exhibit some common structures, such as a hot zone at the up-left of the field of view, and a cold pattern at the bottom-right. It is clear that a more accurate sampling of the rotor temporal period should provide more precise information on the unsteady features, and would allow a more detailed comparison with thermocouple stationary maps.

4. CONCLUSIONS AND PERSPECTIVES

In conclusion, spontaneous rotational Raman thermometry has provided a reliable data set sampling the temperature distribution across three different planes of interest in a turbomachine test rig. Raman temperature maps are compared to thermocouple measurements with due account for the Mach number distribution and for unsteadiness of the flow in the measurement plane. Upstream from the stator, steady state temperature distribution exhibits a clear signature of the swirlers upstream; between the rotor and the stator, the influence of the

two combustor clocking positions (Passage and Leading Edge) were evidenced in the static temperature distribution. Downstream from the rotor, measurements in the stationary and rotating frame are compared. Information on the unsteady behavior of the flow is retrieved by synchronizing the laser pulse train with the rotor clock. In particular, fast temperature variation within one fraction of rotor cycle is probed with 10 µs temporal resolution, revealing a 12 K amplitude modulation.

A more accurate sampling of the rotor period is now necessary to allow full comparison between the steady state measurements and the instantaneous Raman measurements. It could be the purpose of a future work in which an accurate investigation of the Raman signal versus delay between the rotor clock and the laser pulses can be carried out in finer steps along a line or a plane. To go further, a larger angular Raman field of view may be used. This would allow measurements over a full combustor angular period. To do so, cylindrical windows should be used. Moreover, a fully redesigned optical setup, including fibered excitation and collection paths, might be compact enough to be mounted on a rotation platform, to allow the annular scan of the measurement volume.

ACKNOWLEDGEMENTS

The authors thank the NG-Turb facility operation team from DLR for their concern and help to make the experimental campaign a success. Pr. Frederic Grisch from Coria is gratefully acknowledged for fruitful technical discussions. This work was done with the financial support of the European Commission within the FP7 FACTOR project under the Grant Agreement no. 265985.

REFERENCES

[1] A. Alexiou, K. Mathioudakis, *Proc. of ASME Turbo Expo 2005: Power for Land, Sea, and Air* **2005** ; 185.

[2] A. Ehn, J. Zhu, X. Li, J. Kiefer, *Appl. Spectrosc.* **2017** ; 71, 341.

[3] A. C. Eckbreth, *Laser diagnostics for combustion temperature and species,* Gordon and Breach, Amsterdam, **1996**.

[4] D. A. Long, *Raman Spectroscopy*, Cas-Gaw Hill, **1977**.

[5] A. Weber, *Raman spectroscopy of gases and liquids*. Springer Verlag, **1979**.

[6] R. W. Dibble, A. R. Masri, and R.W. Bilger, *Combust. Flame*, **1987** ; 67, 189.

[7] R. Berreby, A. Le Guevel, F. Grisch, *Proc. of ASME Turbo Expo,* **2001**.

[8] R. J. Locke, M. P. Wernet, R. C. Anderson, *Meas. Sci. Technol.*, **2018** ; 29, 015205.

[9] H. Ajrouche, P. Vervisch, A. Lo, A. Cessou, *17th International Symposium on Applications of Laser Techniques to Fluid Mechanics*, **2014**.

[10] M. C. Drake, C. Asawaroengchai, D. L. Drapcho, K. D. Veirs, G. M. Rozenblatt, *AIP Conf. Proc.*, **1982**; 621.

[11] M. C. Drake, G. M. Rozenblatt, *Combust. Flame*, **1978** ; 33, 179.

[12] Y. Gu, E.W. Roth, G.P. Reck , *J. Raman Spectrosc.*, **1997** ; 28, 605-612.

[13] J. M. Fernandez, A. Punge, G. Tejeda, S. Montero, *J. Raman Spectrosc.*, **2006** ; 37, 175.

[14] Y. F. Arshinov, S. M. Bobrovnikov, V. E. Zuev, V. M. Mitev, *Appl. Opt.*, **1993**; 32, 2758.

[15] A. Behrendt, T. Nakamura, M. Onishi, R. Bumgart, T. Tsuda, *Appl. Opt.*, **2002** ; 36, 7657.

[16] S. Y. Chen, Z. J. Qiu, Y. C. Zhang, H. Chen, Y. Wang, *J. Quant. Spectrosc. Radiat. Transfer*, **2011**; 112, 304.

[17] M.P. Thariyan, A. H. Bhuiyan, S. E. Meyer, S. V. Naik, J. P. Gore, R. P. Lucht, *Meas. Sci.Technol.*, **2010** ; 22, 015301.

[18] O. Keck, W. Meier, W. Stricker, M. Aigner, *Combust. Sci. Technol.*, **2002** ; 174, 117.

[19] J. Kojima, Q.-V. Nguyen, *Meas. Sci.Technol*, **2004** ; 15, 565.

[20] J. Kojima and Q.-V. Nguyen, *Meas. Sci.Technol.*, ***2008 ;*** 19, 015406.

[21] M. C. Weikl, F. Beyrau, J. Kiefer, T. Seeger, A. Leipertz, *Opt. Lett.*, **2006** ; 31, 1908.

[22] X.R. Duan, W. P. Weig, B. Lehmann, *Appl. Phys. B*, **2005** ; 80, 389.

[23] E. Dick, *Fundamentals of Turbomachines*, Springer, **2015**.

[24] W. F. Colban, K. A. Thole , G. Zess, *J. Turbomach.*, **2003** ; 125, 193.

[25] W. F. Colban, K. A. Thole , G. Zess, *J. Turbomach.*, **2003** ; 125, 203.

[26] H.-J. Rehder, A. Pahs, M. Bittner, F. Kocian, *ASME Turbo Expo 2017*, **2017**, V02AT40A025.

[27] A. Krumme, M. Tegeler, S. Gattermann, *Proc. of ETC13*, **2019** ; 8.

SUPPORTING INFORMATION

1. DESCRIPTION OF THE FACTOR TEST RIG

Illustrations of the core of the rig structure are given in Fig. S1 (a) and (b)**.** It is based on a rotating turbine test rig with non-reacting combustion simulator, which enables continuous operational testing at relevant Reynolds and Mach numbers. The inlet temperature is 451 K with pressure of 143 kPa while outlet pressure is 53 kPa. Accessing the optical windows was a challenging issue since a containment shield (Fig. S1 (c)) was designed and placed around the rig as a shield in case of failure. A specific tunnel was thus designed into it to allow placing the Raman lens as close as possible from the windows and maximizing the collection solid angle of the Raman backscattering.

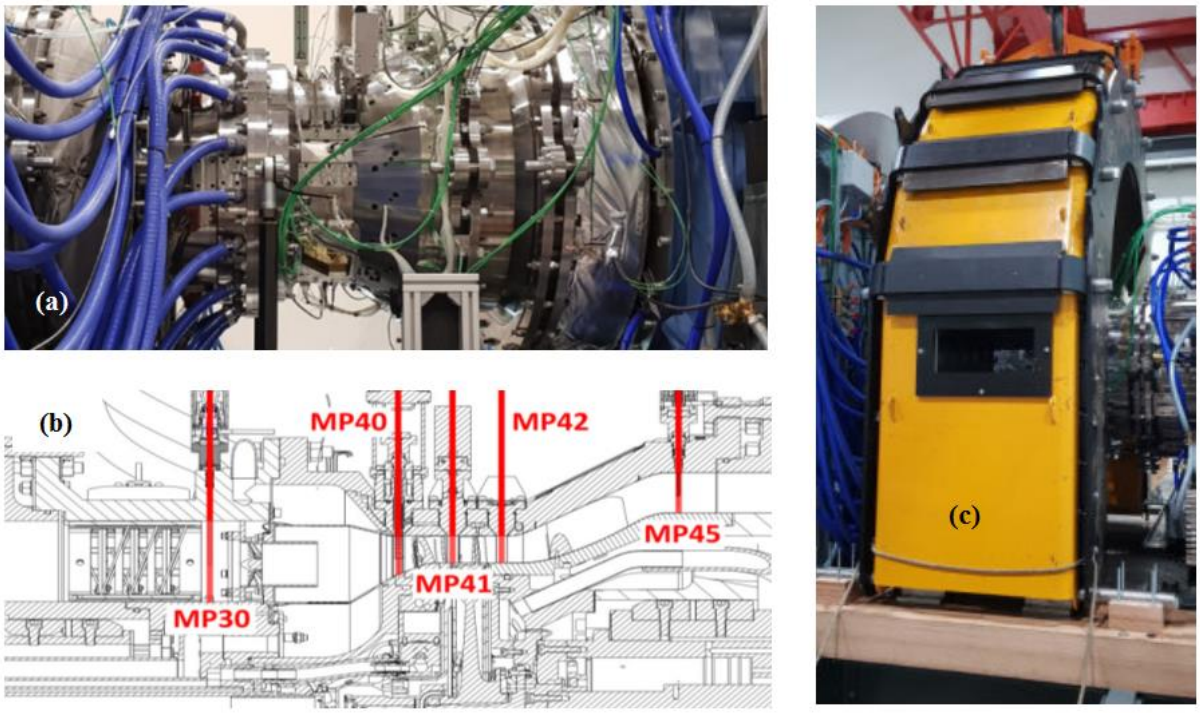

Fig. S1 (a) FACTOR rig photo and (b) CAD cut-away view with indicated probe access measurement planes. (c) Picture of the containment structure placed around the rig with access for laser optics.

2. SIGNAL ACQUISITION

- Temporal synchronization

Synchronization of the laser pulse train to the rotor was achieved through precise timing management as described in Fig. S2. The rotor is operated at 7700 rpm and is formed of 60 identical blades periodically disposed. The laser pulse repetition rate is fixed to 7700 Hz (period τ =130 µs) and locked to the rotor clock in order to keep the measurement volume at a constant position with respect to the rotating blade. To do so, the measured rotor clock was multiplied by 60 using FPGA which is used to trigger the laser through a delay generator. The relative phase between the rotor and laser clocks is scanned by adjusting the delay of the laser trigger. The jitter is calculated for a steady state operation of the rotor. The re-phasing of the laser clock with the rotor blade is achieved at each rotor revolution, i.e. every 60 laser shots.

Considering a variation of the rotation speed smaller than 0.1%, as measured experimentally, the corresponding phase variation is thus estimated to be inferior to $60 * \frac{2\pi}{1000} = \frac{2\pi}{17}$ rad. The phase averaging effect is thus smaller than the sampling time interval ($10\ \mu s \equiv \frac{2\pi}{13} rad$) of the plot of temperature versus delay given in fig.5. Jitter effect is thus neglected in the data analysis. In addition, local fluctuations induced by turbulence cannot be observed here since it may differ from one blade to the other, and our measurement is averaging over all the blades.

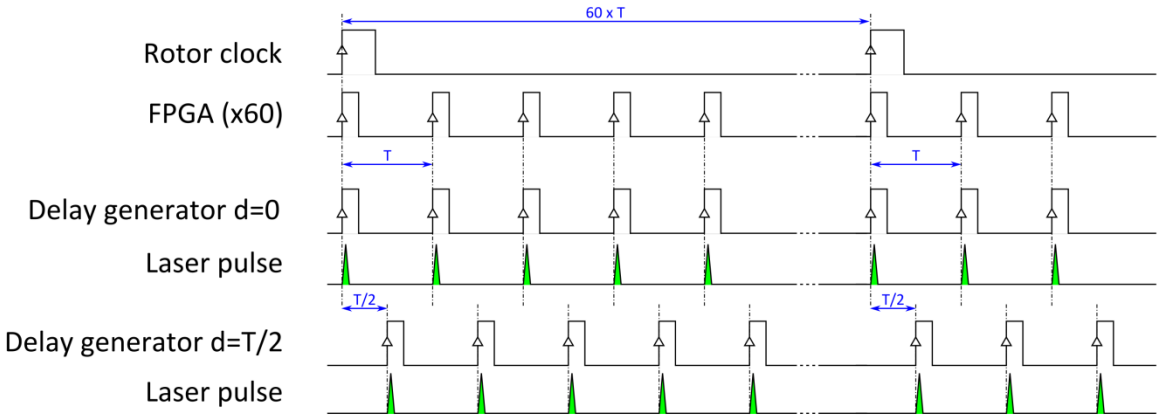

Fig. S2 Synchonization of the laser pulse train to the rotor clock.

- Time integration

Integration time has been fixed to 60 s as it provides good enough signal to noise ratio (SNR) and leads to a ~2 K precision at the center of the chamber. The evolution of the SNR versus integration time is shown in Fig. S3. SNR increases as the square root of the accumulated number of shots, as illustrated by the fitted curve (green line). It thus demonstrates that the measurement is not limited yet by the detector noise and may still improve by increasing integration time.

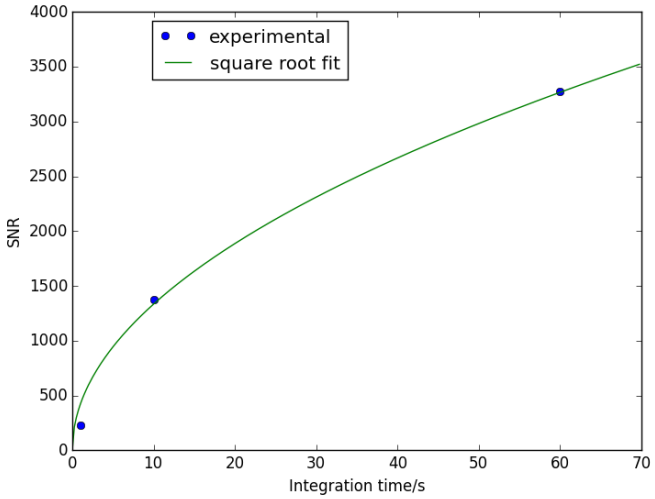

Fig. S3 Signal to noise ratio (SNR) as a function of integration time.

- Mapping of the measurement planes

The mapping is done thanks to a XYZ translation stage, where X is the horizontal axis (orthogonal to the flow), Y is the vertical axis, and Z is the flow direction. The XY mapping of each measurement plane is done by sampling the area every 4 mm (total range of 36 mm) along the horizontal axis X and every 2 mm (total range of 14 mm) along the vertical axis Y. Near the edges of the chamber, a 2 mm minimal distance is set between the measurement volume and the walls in order to avoid spurious light in the detector. Along the vertical axis, the windows diameter is 16 mm (1 mm margin is taken beside the laser beam). Temperature maps are displayed in polar coordinates with an origin at the center of rotation of the rig. A reduced radial coordinate, defined by a zero value at the inner wall of the structure (r=226 mm for MP40 and MP41) is used.

3. COMPARISON BETWEEN RAMAN AND THERMOCOUPLE MEASUREMENTS.

Raman and thermocouple techniques provide different quantities that must be carefully compared. Raman technique is non-invasive and provides a measurement of the static temperature T_{static} of the gas, whereas thermocouple is intrusive and gives a total air temperature T_{total}. The relationship between the two quantities is given by:

$$\frac{T_{total}}{T_{static}} = 1 + \frac{\gamma - 1}{2} {M_a}^2 \qquad (4)$$

where γ is the adiabatic coefficient of the gas (γ=1.4 for dry air), and M_a is the Mach number. Table S1 shows the influence of the mean Mach number value on the ratio T_{static}/T_{total}. The mean total temperature $\langle \mathrm{T_{total}} \rangle$ is used here to calculate the mean correction $\Delta T = |T_{static} - T_{total}|$. The two quantities are thus assumed to be equal for MP40, whereas Mach number corrections have to be taken into account for MP41 and MP42.

Raman measurement section is 90° rotated compared to the thermocouple one. The angular periodicity of the swirlers, stator and rotor are respectively 18°, 9° and 6°, which are 90°-divisors, so the two measurement zones can be considered as conjugated. Finally, the thermocouple is probing over 35°, whereas Raman diagnostic is restricted by optical windows to a 3° angular range of measurement.

Plane	Mach number	T_{static}/T_{total}	$\langle T_{total} \rangle$ (K)	ΔT (K)
40	0.13	0.996	450	1.5
41	0.88	0.865	350	54
42	0.4	0.968	350	11

Table S1. Influence of the Mach number on the averaged total temperature in the three planes of interest**.**

In practice, the Mach number has been measured in each point, simultaneously with the temperature, by the 5-hole probe. Thus the Mach number distribution was used to correct the measurements map measured by the thermocouple in order to compare it to the Raman.